THIRD EUROPEAN ROTORCRAFT AND POWERED LIFT AIRCRAFT FORUM

Paper No. 24

EFFECT OF MODERATE DEFLECTIONS ON THE AEROELASTIC STABILITY OF A ROTOR BLADE IN FORWARD FLIGHT

J. Shamie and P. Friedmann
Mechanics and Structures Department
University of California at Los Angeles
Los Angeles, California, 90024, U.S.A.

September 7-9, 1977

AIX-EN-PROVENCE, FRANCE

ASSOCIATION AERONAUTIQUE ET ASTRONAUTIQUE DE FRANCE

EFFECT OF MODERATE DEFLECTIONS ON THE AEROELASTIC STABILITY OF A ROTOR BLADE IN FORWARD FLIGHT*

J. Shamie, Postdoctoral Scholar
and
P. Friedmann, Associate Professor
Mechanics and Structures Department
School of Engineering and Applied Science
University of California
Los Angeles, California 90024 U.S.A.

ABSTRACT

The derivation of a system of general, nonlinear coupled flap-lag-torsional equations of motion for moderately large deformations of an elastic rotor blade, in forward flight, are described. The aeroelastic stability of the blade in forward flight is investigated using a linearized system of equations of motion. The equilibrium position about which the equations are linearized is obtained by considering the trim state of the helicopter, in true or simulated forward flight conditions.

1. Introduction

In recent years the hingeless rotor, in which the blades are cantilevered to the hub, has become an increasingly attractive concept due to its mechanical simplicity of construction and favorable control characteristics. A number of successful hingeless rotored helicopters have been built and are in service, both in military and civilian applications, clearly indicating that the hingeless rotor is starting to fulfill its initial promise. A growing acceptance of hingeless rotor systems for conventional helicopters flying at high speeds has intensified the need for additional fundamental research in this area of rotary-wing aeroelasticity.

Recent research[1] has clearly indicated that the fundamental problem in rotary-wing aeroelasticity is the coupled flap, (out of plane of rotation bending), lead-lag, (inplane of rotation bending) and torsional aeroelastic problem[1-10]. Another aspect of the rotary-wing aeroelastic problem which has recently gained wide acceptance is the fact that rotary-wing aeroelasticity is inherently nonlinear.[1] Thus the correct treatment of a wide class of problems in this area requires a consistent development of a mathematical model, for the particular aeroelastic problem being considered, which results

*This work was supported by Langley Directorate, U.S. Army Air Mobility Research and Development Laboratory and NASA Langley Research Center, Hampton, Virginia under NASA NGR 05-007-414.

in a system of nonlinear equations of motion.[1-10] The nonlinear terms in these equations are due to the inclusion of moderately large deflections in the elastic, inertial and aerodynamic operators of this aeroelastic problem. Physically these moderately large deflections correspond to a situation where one has small elastic strains combined with finite rotations (large slopes).

The coupled flap-lag-torsional equations of motion for a single blade are the basic building blocks from which the more complicated aeroelastic problems such as the coupled rotor/fuselage or the coupled rotor/fuselage/control system formulations can be developed.[1]

During the past few years a number of equations for the coupled flap-lag-torsional motion of hingeless rotor blades have been derived by a number of authors.[3,4,6-14]

A fundamental set of equations for blades having no droop, sweep and precone has been derived by Houbolt and Brooks.[6] All three flap, lag and torsional degrees of freedom were taken into account, the final equations obtained were intended to represent only the linear problem. Furthermore the aerodynamic loading terms were left in a general unspecified form.

Following this work other researchers presented derivations of equations of motion which included additional nonlinear terms, due to moderately large deflections, in the structural inertia and aerodynamic operators of this aeroelastic problem.[3,4,6-14]

The basic geometry and parameters of a general hingeless rotor blade are illustrated in Figures 1A and 1B. Figures 2 and 3 illustrate various geometric aspects of the blade configuration which is the subject matter of this paper.

A number of studies have derived equations capable of simulating the motion of this configuration with varying degrees of sophistication. The equations developed by Hodges and Dowell,[8,9] and more recently by Hodges and Ormiston are capable of simulating the complete coupled flap-lag-torsional motion of a rotor blade with, distributed torsion, variable structural coupling, precone and no offset between elastic axis, the aerodynamic center and cross-sectional center of mass. Furthermore, the aerodynamic and inertia loads corresponding to these equations are restricted to the case of hover. A recently derived version of these equations, described in a preliminary report by Hodges,[14] has been generalized to include the effects of pitch link flexibility, twist, precone, droop, sweep and torque offsets. However, the equations are still restricted to the case of hover and have no capability of simulating the various cross-sectional offsets between elastic axis, aerodynamic center and cross-sectional center of mass shown in Figure 1B (which occur in practice). Furthermore these equations are also restricted to the case of uniform mass and stiffness distribution. Some solutions to these equations showing the effects of precone, droop and pitch link flexibility were presented in Reference 10.

Another set of equations derived by Friedmann and Tong[3] has undergone considerable modification[7] so that it could simulate the coupled flap-lag-torsional motion of blades having built in twist, precone, distributed torsion and root torsion (or pitch link flexibility) and offsets between aerodynamic center, elastic axis and blade cross-sectional center of mass, shown in Figure 1B. The aerodynamic loads presented with these equations[7] were also limited to the case of hover.

Another advanced and comprehensive set of equations of motion aimed at modeling a particularly complicated composite bearingless rotor blade has been recently developed by Bielawa.[11,12] These equations which are applicable to both hover and forward flight are intended to model structural redundancies and nonlinear twist present in the bearingless, hingeless rotor and were not intended to simulate conventional, arbitrary hingeless blade configurations.

Another relatively general set of equations of motion has been presented in Reference 13. These equations are capable of simulating the coupled flap-lag-torsional dynamics of a blade having: precone, droop, pretwist, distributed torsion, root torsion (or pitch link flexibility), various blade root offsets and also offsets between the elastic axis, aerodynamic center and the blade cross-sectional center of mass shown in Figure 3. Furthermore the aerodynamic loads derived for these equations are applicable to both the case of hover and forward flight.[13] Detailed solutions to these equations for the case of hover were presented by Powers.[15] Typical results illustrating the coupled flap-lag-torsional dynamics in forward flight were presented in Reference 16. The main emphasis in Reference 16 was the comparison of the results obtained including the effect of forward flight with results obtained previously for the case of hover. Furthermore the results presented in Reference 16 can be also viewed as an extension of previously published coupled flap-lag results in forward flight[17] to the case of complate coupled flap-lag-torsion. The most important conclusions presented in Reference 16 were: (a) significant degradation in blade stability margins can occur due to forward flight and (b) the torsional dynamics are very important for the correct modeling of rotor blades in forward flight.

Recently a general set of nonlinear equations of equilibrium for elastic helicopter blades undergoing moderate deformations has been derived by Rosen and Friedmann.[18] These equations are general and the loads associated with the inertia and aerodynamic operators of this aeroelastic problem are left unspecified and presented in a general symbolic form. The most important and convenient feature of these equations is the fact that they are more consistent than the equations which have been used previously.[3,7,13]

The present paper has a number of objectives. First, starting from the general equations given in Reference 18, the inertia and aerodynamic operators will be derived for the case of coupled flap-lag-torsional dynamics of a rotor blade in forward flight. Next some typical results for stability boundaries in forward flight will be presented and differences between these results on previous results[16] are identified and discussed.

Finally the importance of the time dependent equilibrium position about which the equations of motion are linearized will be illustrated by comparing stability boundaries which are obtained by linearizing the equations about an approximate, linear, time equilibrium position with the aeroelastic stability boundaries obtained by linearizing the equations about a nonlinear, more accurate, time dependent equilibrium position.

2. Brief Description of the Equations of Motion

2.1 General

The structural part of the equations of motion upon which this study is based are described in detail in Reference 18. As shown in Reference 18 only a limited number of assumptions are required in this derivation, when the inertia and aerodynamic loads are written in a general symbolic form. When deriving aerodynamic and inertia loads consistent with these equations additional assumptions are required and a more detailed ordering scheme has to be stipulated. These ingredients, together with the final partial, nonlinear, differential equations describing the coupled flap-lag-torsional aeroelastic problem in forward flight are presented in the following sections. Due to the relatively cumbersome nature of these equations the presentation will be concise. Additional details will be available in Reference 19.

2.2 Assumptions and Ordering Scheme Used in the Aeroelastic Analysis

2.2.1 Assumptions

The geometry of the problem is shown in Figures 1, 2, and 3. The following assumptions were used in the treatment of the coupled flap-lag-torsional aeroelastic stability problem in forward flight: (a) the blade is initially straight and has no angle of sweep, droop or torque offset (see Fig. 1). The blade is cantilevered at the hub, its feathering axis is preconed by an angle β_p which is assumed to be small. Furthermore the blade root is offset by a distance e_1 from the axis of rotation (b) the blade has an angle of built in twist $\theta_B(\bar{x})$, occuring about the undeformed elastic axis. An additional contribution to the total pitch angle of the blade is due to the collective and cyclic pitch contributions given by

$$\theta_r = \theta_0 + \theta_{1c} \cos\psi + \theta_{1s} \sin\psi \qquad (1)$$

(c) cross section of the blade is symmetrical with respect to the major principal axis of the cross section (d) the blade cross sectional center of gravity (C.G.), aerodynamic center (A.C.) and elastic axis (E.A.) are distinct points. However the blade cross sectional area centroid and elastic axis are assumed to be coincident (e) the blade is built of an isotropic, linearly elastic material (f) during the deformation the Euler-Bernoulli assumption is used, i.e., cross sections remain plane and normal to the deformed elastic axis; that is the effect of shear deformation is neglected (g) the blade can bend in two mutually perpendicular directions. The torsional deformations of the blade consist of two parts: distributed torsional elastic deformation ϕ_D which occurs about the deformed elastic

axis of the blade and root torsional deformation ϕ_R, due to pitch link flexibility or control system stiffness K_ϕ, which is assumed to occur about the feathering axis of the blade (h) the blade is assumed to have moderate deflections, which implies small strains and finite rotations or slopes. These elastic rotations are assumed to be of order ε_D ($\varepsilon_D \tilde{=} 0.20$) so that terms of $0(\varepsilon_D^2)$ are negligible compared to terms of order one, 0(1). (i) structural damping forces are assumed to be of a viscous type (j) the blades are attached to an aircraft of infinite mass and no coupling between the blade and fuselage degrees of freedom exists. Hence the stability of a single blade can represent the aeroelastic properties of the complete rotor (k) the blade is rotating at constant angular speed Ω, furthermore the helicopter is flying at a constant speed of forward flight V. (ℓ) two dimensional quasi-steady aerodynamic loads are used and apparent mass terms are neglected. Furthermore compressibility and stall are also neglected. A detailed discussion of the importance of some of these assumptions in rotary wing aeroelasticity, for the case of hover,were given in Reference 20 (m) the effect of reversed flow is included in the calculations in an exact manner[21] (n) the representation of the inflow in the aerodynamic loads is general having the functional form given by

$$\lambda = \lambda_0 k_1(\bar{x}) + \lambda_{1c}\, k_2(\bar{x})\, \cos\psi + \lambda_{1s} k_3(\bar{x})\, \sin\psi \qquad (2)$$

2.2.2 The Ordering Scheme

The flutter boundaries obtained in this study are based upon a system of linearized equations of motion from which the dynamic stability of the rotor blade in forward flight is determined. The linearized aeroelastic equations are obtained by first deriving a set of nonlinear equations which are subsequently linearized in a consistent manner. The nonlinear equations are obtained by introducing the assumption of moderate elastic deformations, which implies that strains are small and negligible compared to terms of order one, while elastic slopes are of order ε_D ($\varepsilon_D = 0.20$) and terms containing the squares of the slopes are neglected when compared to terms of order one, i.e.

$$0(1) + 0(\varepsilon_D^2) \tilde{=} 0(1) \qquad (3)$$

In the process of deriving these nonlinear equations a considerable number of small terms are encountered; several of these terms are neglected by assigning an order of magnitude, in terms of a typical elastic slope ε_D, to each important parameter in the problem. Equations of manageable size are obtained by applying assumption (h) of the previous section. The orders of magnitude assigned to the various parameters in this study are given below:

$$(u/\ell) = 0(\varepsilon_D^2)\ ;\quad \partial w/\partial x = \partial v/\partial x = \phi = \beta_p = \lambda_o = 0(\varepsilon_D)$$

$$(x/\ell) = \mu = \partial/\partial\psi = \bar{x}_A = \partial/\partial\bar{x} = 0(1)$$

$$\lambda_{1c} = \lambda_{1s} = b = 0(\varepsilon_D)\ ;\ C_{do}/a = \bar{x}_I = 0(\varepsilon_D^2)$$

$$\theta_0 = \theta_{1c} = \theta_{1s} = 0(\varepsilon_D^{1/2})\ ;\quad \bar{k}_{m2} = \bar{k}_{m3} = 0(\varepsilon_D^2)$$

The main advantage from using an ordering scheme, such as described above, is the ability to neglect higher order terms in a systematic manner, so as to obtain a set of simplified equations which contain the most important terms governing this aeroelastic problem. It should be noted however that since the ordering scheme is primarily a result of a combination of experience and common sense it should be used with a certain degree of flexibility so as to enable one, when necessary, to retain certain higher order terms even though they may appear negligible when considered strictly in the light of the ordering scheme.

2.3 The Equations of Motion

This study is based upon a set of consistently derived, nonlinear partial differential equations describing the coupled flap-lag-torsional dynamics of an isolated rotor blade in forward flight. A general version of these equations, with the inertia and aerodynamic loads left in a general symbolic form has been presented in Reference 16. These general equations of equilibrium which serve as the starting point in this study are given below:

$$T_{,x} + (v_{,x}\tilde{q}_z)_{,x} - (w_{,x}\tilde{q}_y)_{,x} + \tilde{p}_x = 0 \tag{4}$$

$$-[E(I_2\cos^2\theta_G + I_3\sin^2\theta_G)v_{,xx} + E(I_2-I_3)\phi w_{,xx}\cos 2\theta_G$$

$$+E(I_2-I_3)\sin\theta_G\cos\theta_G(w_{,xx}-2\phi v_{,xx})-Tx_{II}(\cos\theta_G-\phi\sin\theta_G)]_{,xx}$$

$$-(GJ\phi_{,x}w_{,xx})_{,x} + (v_{,x}T)_{,x} + (w_{,x}\tilde{q}_x)_{,x} - \tilde{q}_{z,x} + \tilde{p}_y = 0 \tag{5}$$

$$-[E(I_2-I_3)\sin\theta_G\cos\theta_G(v_{,xx} + 2\phi w_{,xx}) + E(I_2\sin^2\theta_G +$$

$$I_3\cos^2\theta_G)w_{,xx} + E(I_2-I_3)\phi v_{,xx}\cos 2\theta_G - Tx_{II}(\sin\theta_G+\phi\cos\theta_G)]_{,xx}$$

$$+(GJ\phi_{,x}v_{,xx})_{,x} + (w_{,x}T)_{,x} - (v_{,x}\tilde{q}_x)_{,x} + \tilde{q}_{y,x} + \tilde{p}_z = 0 \tag{6}$$

$$[GJ(\phi_{,x} + v_{,xx}w_{,x})]_{,x} + E(I_2-I_3)[(v^2_{,xx}-w^2_{,xx})\sin\theta_G\cos\theta_G$$

$$-v_{,xx}w_{,xx}\cos 2\theta_G] + Tx_{II}\,(w_{,xx}\cos\theta_G - v_{,xx}\sin\theta_G)$$

$$+\tilde{q}_x + v_{,x}\tilde{q}_y + w_{,x}\tilde{q}_z = 0 \tag{7}$$

The last three equations represent respectively blade equilibrium in the lagwise, flapwise and torsional degrees of freedom. These equations

are written in the undeformed coordinate system, furthermore according to assumption (d) the offset $x_{II} = 0$, in the present study.

The distributed force and moment vectors per unit length of the undeformed elastic axis may be expressed as

$$\bar{p} = \tilde{p}_x \hat{e}_x + \tilde{p}_y \hat{e}_y + \tilde{p}_z \hat{e}_z \tag{8}$$

$$\bar{q} = \tilde{q}_x \hat{e}_x + \tilde{q}_y \hat{e}_y + \tilde{q}_z \hat{e}_z \tag{9}$$

These general loading vectors consist of three contributions, inertia loads, aerodynamic loads and damping loads which are symbolically represented by

$$\bar{p} = \bar{p}_I + \bar{p}_A + \bar{p}_D \tag{10}$$

$$\bar{q} = \bar{q}_I + \bar{q}_A + \bar{q}_D \tag{11}$$

The derivation of the inertia, aerodynamic and damping loads per unit length is described briefly below, additional details can be found in Reference 19.

Inertia Loads are obtained by using elementary mechanics[22] to derive the acceleration vector for a mass point in the blade, rotating with constant angular speed

$$\bar{a} = \ddot{\bar{R}} + 2\,\bar{\Omega} \times \dot{\bar{R}} + \bar{\Omega} \times (\bar{\Omega} \times \bar{R}) \tag{12}$$

where $$\bar{R} = e_1 \underset{\sim}{i} + (x_0 + u)\hat{e}_x + v\hat{e}_y + w\hat{e}_z + y_0 \hat{e}'_y + z_0 \hat{e}'_z \tag{13}$$

$$\bar{\Omega} = \Omega \underset{\sim}{k} \tag{14}$$

the various unit vectors, or coordinate systems used are shown in Figures 2 and 3, and the transformations between them are given by

$$\hat{e}_x = \cos\beta_p \underset{\sim}{i} + \sin\beta_p \underset{\sim}{k}$$

$$\hat{e}_y = \underset{\sim}{j}$$

$$\hat{e}_z = -\sin\beta_p \underset{\sim}{i} + \cos\beta_p \underset{\sim}{k} \tag{15}$$

and

$$\hat{e}'_x = \hat{e}_x + v_{,x}\hat{e}_y + w_{,x}\hat{e}_z$$

$$\hat{e}'_y = -(v_{,x} + \phi w_{,x})\hat{e}_x + \hat{e}_y + \phi\hat{e}_z$$

$$\hat{e}'_z = =(w_{,x} - \phi v_{,x})\hat{e}_x - (\phi + v_{,x}w_{,x})\hat{e}_y + \hat{e}_z \tag{16}$$

The last transformation, Equation (16) represents the relation between the deformed and undeformed coordinates of the blade, which has been derived in Reference 18. Use of Eqs. (12) through (16), applying D'Alembert's principle and using the ordering scheme presented in the previous section yields

$$\bar{p}_I = \tilde{p}_{xI}\hat{e}_x + p_{yI}\hat{e}_y + p_{zI}\hat{e}_z = -\int_A \rho \bar{a} dA \tag{17}$$

$$\tilde{p}_{xI} = m\Omega^2(2\overset{*}{v} + x_0 + e_1) \tag{18}$$

$$\tilde{p}_{yI} = m\Omega^2(-\overset{**}{v} - 2\overset{*}{u} + 2\overset{*}{w}\beta_p + v + x_I\cos\theta_G + x_I\overset{**}{\theta}_G\sin\theta_G) \tag{19}$$

$$\tilde{p}_{zI} = m\Omega^2[-\overset{**}{w} - 2\overset{*}{v}\beta_p - \beta_p(x_0 + e_1) - x_I\overset{**}{\theta}_G\cos\theta_G] \tag{20}$$

$$\text{where} \quad \theta_G = \theta_B(\bar{x}) + \theta_r \tag{21}$$

$$u = -\tfrac{1}{2}\int_0^{x_0}[(v_{,x})^2 + (w_{,x})^2]dx \tag{22}$$

Equation (22) represents the assumption that the blade is inextensional in the axial direction which is commonly made in rotary wing aeroelasticity.

The inertia moment per unit span of the blade is given by

$$\bar{q}_I = -\int_A \rho\, \bar{R}_p \times \bar{a} dA = \tilde{q}_{xI}\hat{e}_x + q_{yI}\hat{e}_y + \tilde{q}_{zI}\hat{e}_z \tag{23}$$

$$\text{where} \qquad \bar{R}_p = y_0\hat{e}'_y + z_0\hat{e}'_z \tag{24}$$

Substitution of the Eqs. (13), (16) and (24) into Eq. (23) yields lengthy expressions[19] for $\tilde{q}_{xI}$, $\tilde{q}_{yI}$ and $\tilde{q}_{zI}$. Fortunately when these terms are substituted into Eqs. (4) through (7), and the ordering scheme is used,

a considerable number of small terms can be neglected. Thus, while detailed expressions for q_{xI}, q_{yI} and q_{yI} and q_{zI} are not presented in this paper, it should be understood that the final equations of motion in partial differential form, given at the end of this section, contain all the non-negligible contributions of the distributed inertia moments per unit span.

Aerodynamic Loads The aerodynamic loads and moments are calculated using an interpretation of fixed wing quasisteady aerodynamics which is similar to conventional blade element theory. It should be emphasized that the application of any unsteady aerodynamic theory to rotor blades has to be done carefully and will usually require the introduction of certain small and not very significant, approximations[20].

The important ingredient required for the calculation of the aerodynamic loads is the velocity vector at the elastic axis of the blade given by

$$\underset{\sim}{V}_{EA} = \dot{\bar{R}}_{EA} + \bar{\Omega} \times \bar{R}_{EA} \tag{25}$$

where $\bar{R}_{EA}$ is given by Eq. (13) when $y_0 = z_0 = 0$. Using the hubplane coordinate system, and small angles of precone one has

$$\bar{R}_{EA} = (x_0 + u + e_1 - w\beta_p)\underset{\sim}{i} + v\underset{\sim}{j} + [(x_0 + u)\beta_p + w]\underset{\sim}{k} \tag{26}$$

combining Eqs. (24) and (25)

$$V_{EA} = \Omega(\overset{*}{v} - \overset{*}{w}\beta_p - v)\underset{\sim}{i} + \Omega(\overset{*}{\bar{v}} + x_0 + e_1)\underset{\sim}{j} + \Omega\overset{*}{w}\,\underset{\sim}{k} \tag{27}$$

In order to calculate the aerodynamic loads the velocities of the blade elastic axis, in the deformed coordinate system are required. Thus Eq. (15) has to be used together with the inverse of the transformation[18] represented by Eq. (16)

$$\begin{aligned}
\hat{e}_x &= \hat{e}'_x + S_{21}\,\hat{e}'_y + S_{31}\,\hat{e}'_z \\
\hat{e}_y &= S_{12}\,\hat{e}'_x + \hat{e}'_y + S_{32}\,\hat{e}'_z \\
\hat{e}_z &= S_{13}\,\hat{e}'_x + S_{23}\,\hat{e}'_y + \hat{e}'_z
\end{aligned} \tag{28}$$

where[18]

$$S_{12} = v_{,x} \; ; \; S_{21} = -(v_{,x} + \phi w_{,x}) \; ; \; S_{13} = w_{,x}$$

$$S_{23} = \phi \; ; \; S_{31} = -(w_{,x} - \phi v_{,x}) \; ; \; S_{32} = -(\phi + v_{,x} w_{,x}) \qquad (29)$$

Substitution of Eqs. (15), (28) and (29) into Eq. (27) and applying the ordering scheme yields an expression for $\underset{\sim}{V}_{EA}$ in the deformed $\hat{e}'_x$, $\hat{e}'_y$ and $\hat{e}'_z$ coordinate system

$$\underset{\sim}{V}_{EA} = \Omega[\overset{*}{u} - \overset{*}{w}\beta_p + v) + (\overset{*}{v} + x_0 + e_1)w_{,x} + \overset{*}{w}(\beta_p + w_{,x})]\hat{e}'_x$$

$$+ \Omega(\overset{*}{v} + x_0 + e_1)\hat{e}'_y + \Omega[vw_{,x} + v\beta_p - \overset{*}{v}\phi -$$

$$- (x_0 + e_1)(\phi + v_{,x}w_{,x}) + \overset{*}{w}]\hat{e}'_z \qquad (30)$$

In addition to the contribution to the velocity vector resulting from the deformation of the blade and its rotation, another contribution due to inflow[17,19,21] has to be also taken into account. This contribution to the velocity can be written as

$$\underset{\sim}{V}_A = \mu\Omega R \cos\psi \; \underset{\sim}{i} - \mu r R \sin\psi \; \underset{\sim}{j} - \Omega R\lambda \underset{\sim}{k} \qquad (31)$$

Using Eqs. (28) and (29), i.e. transforming to the deformed blade coordinate system, and applying the ordering scheme

$$\underset{\sim}{V}_A = \Omega R(\mu\cos\psi - \mu\sin\psi w_{,x})\hat{e}'_x + \Omega R(-\mu\cos\psi v_{,x} - \mu\sin\psi)\hat{e}'_y$$

$$+ \Omega R[-\mu\cos\psi(w_{,x} - \phi v_{,x} + \beta_p) + \mu\sin\psi(\phi + v_{,x}w_{,x}) - \lambda]\hat{e}'_z \qquad (32)$$

Thus the total velocity felt by a point on the elastic axis of the blade is given by

$$\underset{\sim}{U} = \underset{\sim}{V}_A - \underset{\sim}{V}_{EA} = U'_x \hat{e}'_x + U'_y \hat{e}'_y + U'_z \hat{e}'_z \qquad (33)$$

In two dimensional unsteady, fixed wing, aerodynamics the load and moment per unit span are given by [20,23]

$$L = L_Q C(k) + 0.5\rho_A (bR)^2 [\ddot{h} + V_0\dot{\alpha} - (x_A - 0.5bR)\ddot{\alpha}] \tag{34}$$

$$M = C(k)L_Q x_A + 0.5\rho_A (bR)^3 (x_A - 0.5bR)[\ddot{h} - (x_A - 0.5bR)\ddot{\alpha}]$$

$$- 0.5\rho_A V_0 \dot{\alpha}(bR - x_A)(bR)^2 - (a/16)\rho_A (bR)^4 \ddot{\alpha} \tag{35}$$

where the quasisteady lift is given by

$$L_Q = a\rho_A bRV_0 [V_0\alpha + \dot{h} + (bR - x_A)\dot{\alpha}] \tag{36}$$

For quasisteady aerodynamics Theodorsen's lift deficiency function $C(k) = 1$. Furthermore acceleration type noncirculatory terms, sometimes denoted as apparent mass terms will be also neglected, with the exception of the term representing damping in pitch, as is commonly done in rotary wing aeroelasticity. To apply Eqs. (34) through (36) to the present problem it is convenient to consider a system of unit vectors $\hat{e}''_x$, $\hat{e}''_y$ and $\hat{e}''_z$, where the double prime system is obtained from the deformed blade coordinate system by performing a rotation $-\phi\hat{e}'_x$, that is

$$\begin{Bmatrix} \hat{e}''_y \\ \hat{e}''_z \end{Bmatrix} = \begin{bmatrix} \cos\phi & -\sin\phi \\ \sin\phi & \cos\phi \end{bmatrix} \begin{Bmatrix} \hat{e}'_y \\ \hat{e}'_z \end{Bmatrix} \tag{37}$$

The velocities in the two systems are then related by

$$U''_y = U'_y - \phi U'_z$$

$$U''_z = \phi U'_y + U'_z \tag{38}$$

Next, by identifying the following relations

$$V_0 = -U''_y \; ; \; \dot{h} = U''_z \; ; \; \alpha = \theta_G + \phi \tag{39}$$

the aerodynamic loads and moments per unit span can be written in the following manner

$$L = a\rho_A U''_y bR[U''_y(\theta_G + \phi) - U''_z - (\tfrac{3}{2} - \bar{x}_A)bR(\overset{*}{\theta}_G + \overset{*}{\phi})\Omega] \tag{40}$$

$$P''_{zA} = L\cos\left[\tan^{-1}\left(\frac{U''_z}{U''_y}\right)\right] \tilde{=} L \tag{41}$$

$$P''_{yA} = -L\sin\left[\tan^{-1}\left(\frac{U''_z}{U''_y}\right)\right] - \rho_A bRC_{d0}\left[(U''_y)^2 + (U''_z)^2\right] \tag{42}$$

$$= -\frac{U''_z}{U''_y} L - \rho_A bRC_{d0}\,(U''_y)^2$$

$$q''_{xA} = M = \rho_A a(bR)^2 U''_y\{\bar{x}_A[U''_y(\theta_G+\phi) - U''_z] + (0.5-\bar{x}_A)bR(\dot{\theta}_G+\dot{\phi})\} \tag{43}$$

To obtain the final aerodynamic loads in the undeformed coordinate system, the following transformation has to be used

$$\begin{Bmatrix} p_{xA} \\ p_{yA} \\ p_{zA} \end{Bmatrix} = \begin{bmatrix} 1 & -v_{,x} & -w_{,x} \\ v_{,x} & 1 & -v_{,x}w_{,x} \\ w_{,x} & 0 & 1 \end{bmatrix} \begin{Bmatrix} 0 \\ p''_{yA} \\ p''_{zA} \end{Bmatrix} \tag{44}$$

and similarly

$$\begin{Bmatrix} q_{xA} \\ q_{yA} \\ q_{zA} \end{Bmatrix} = \begin{bmatrix} 1 & -v_{,x} & -w_{,x} \\ v_{,x} & 1 & -v_{,x}w_{,x} \\ w_{,x} & 0 & 1 \end{bmatrix} \begin{Bmatrix} q_{xA} \\ 0 \\ 0 \end{Bmatrix} \tag{45}$$

$\tilde{p}_{xA}$ It should be noted that the aerodynamic load in the $\hat{e}_x$ direction given by Eq. (45) is negligible as shown in Ref. 24.

Substitution of the appropriate velocity components into Eqs. (41) through (43) and use of Eqs. (44), (45) and the ordering scheme, results in the final expressions for the aerodynamic loads[19], which are presented below

$$\tilde{p}_{zA} = a\rho_A bR^3\Omega^2\{(\theta_G + \phi)[2\mu^2 v_{,x}\cos\psi\sin\psi + 2v_{,x}(\bar{x}_0 + \bar{e}_1)(\ell/R)\mu\cos\psi$$

$$+ \mu^2\sin^2\psi + 2\mu\overset{*}{\bar{v}}(\ell/R)\sin\psi + 2\mu(\bar{x}_0 + \bar{e}_1)(\ell/R)\sin\psi$$

$$+ 2\overset{*}{\bar{v}}(\bar{x}_0 + \bar{e}_1)(\ell/R)^2 + (\bar{x}_0 + \bar{e}_1)^2(\ell/R)^2] - \mu^2\cos^2\psi v_{,x}(w_{,x} + \beta_p)$$

$$+ \mu\cos\psi[-v_{,x}\lambda - \overset{*}{\bar{w}}\, v_{,x}(\ell/R) - (w_{,x} + \beta_p)\overset{*}{\bar{v}}(\ell/R) - (w_{,x} + \beta_p)(\bar{x}_0 + \bar{e}_1)\ell/R]$$

$$-\mu^2\sin\psi\cos\psi(w_{,x} + \beta_p) + \underline{\mu^2\sin^2\psi v_{,x}w_{,x}} + \mu\sin\psi[-\lambda -$$

$$-\bar{v}(\ell/R) - \bar{v}(\ell/R)(w_{,x} + \beta_p) - \overset{*}{\bar{w}}(\ell/R) + \underline{2v_{,x}w_{,x}(\ell/R)(\bar{x}_0 + \bar{e}_1)}]$$

$$-\lambda\overset{*}{\bar{v}}(\ell/R) - \overset{*}{\bar{v}}\,\overset{*}{\bar{w}}(\ell/R) - \lambda(\ell/R)(\bar{x}_0 + \bar{e}_1) - \bar{v}(w_{,x} + \beta_p)(\bar{x}_0 + \bar{e}_1)(\ell/R)$$

$$-\overset{*}{\bar{w}}(\bar{x}_0 + \bar{e}_1)(\ell/R) + (\bar{x}_0 + \bar{e}_1)^2(\ell/R)^2 w_{,x}v_{,x} + (1.5 - \bar{x}_A)b\overset{*}{\theta}_G[\mu\sin\psi +$$

$$(\ell/R)(\bar{x}_0 + \bar{e}_1)]\} \qquad (46)$$

$$\tilde{p}_{yA} = -a\rho_A bR^3\Omega^2 \Big\langle (\theta_G + \phi)\{\mu^2\cos^2\psi(v_{,x}w_{,x} + v_{,x}\beta_p)$$

$$+\mu^2\sin\psi\cos\psi(w_{,x} + \beta_p) = \mu\cos\psi[\lambda v_{,x} + v_{,x}\overset{*}{\bar{w}}(\ell/R) + (\ell/R)\overset{*}{\bar{v}}\, w_{,x} +$$

$$\overset{*}{\bar{v}}\beta_p(\ell/R) + (w_{,x} + \beta_p)(\bar{x}_0 + \bar{e}_1)(\ell/R)] + \mu\sin\psi[\lambda + \bar{v}w_{,x}(\ell/R) +$$

$$+ \bar{v}\beta_p(\ell/R) + \overset{*}{\bar{w}}(\ell/R)] + \lambda(\ell/R)\overset{*}{\bar{v}} + \overset{**}{\bar{v}\bar{w}}(\ell/R)^2 + \lambda(\bar{x}_0 + \bar{e}_1)(\ell/R)$$

$$+ \bar{v}(w_{,x} + b_p)(\bar{x}_0 + \bar{e}_1)(\ell/R)^2 + \overset{*}{\bar{w}}(\bar{x}_0 + \bar{e}_1)(\ell/R)^2\}$$

$$-\mu^2\cos^2\psi(w_{,x}{}^2+2w_{,x}\beta_p+\beta_p{}^2)-\mu\cos\psi[2\lambda w_{,x}+2\lambda\beta_p+2w_{,x}{}^2\,\bar{v}(\ell/R)$$

$$+4w_{,x}\beta_p\bar{v}(\ell/R) + 2\beta_p{}^2\bar{v}(\ell/R) + 2w_{,x}\overset{*}{\bar{v}} + 2\beta_p\overset{*}{\bar{w}}]$$

$$-\lambda^2-2\lambda\bar{v}(w_{,x} + \beta_p)(\ell/R)-2\lambda\overset{*}{\bar{w}}(\ell/R)-2\overset{*}{\bar{w}}\,\bar{v}w_{,x}(\ell/R)^2 -$$

$$-2\overset{*}{\bar{w}}\bar{v}\beta_p(\ell/R)^2-\overset{*}{\bar{w}}{}^2(\ell/R)^2 + [\mu\sin\psi +(\bar{x}_0 + \bar{e}_1)(\ell/R)]w_{,x}v_{,x}[\mu\cos\psi(w_{,x}+\beta_p)$$

$$+ \lambda + \overset{*}{\bar{w}}(\ell/R)]-(1.5-\bar{x}_A)b(\overset{*}{\theta}_G + \overset{*}{\phi})[-\mu\cos\psi(w_{,x} + \beta_p)$$

$$- \lambda -\overset{*}{\bar{w}}(\ell/R)]+(C_{d0}/a)[2\mu^2v_{,x}\cos\psi\sin\psi + 2(\ell/R)\mu(\bar{x}_0+\bar{e}_1)v_{,x}\cos\psi$$

$$+ \mu^2\sin^2\psi +2(\ell/R)\mu\sin\psi(\overset{*}{\bar{v}} + \bar{x}_0 + \bar{e}_1)+2(\ell/R)^2\overset{*}{\bar{v}}(\bar{x}_0 + \bar{e}_1) +$$

$$+(\ell/R)^2(\bar{x}_0 + \bar{e}_1)^2]\Big\rangle \qquad (47)$$

$$\tilde{q}_{xA} = \rho_A a(bR)^2R^2\Omega^2\Big\langle \bar{x}_A\{(\theta_G + \phi)[2\mu^2v_{,x}\cos\psi\sin\psi +$$

$$+2v_{,x}(\bar{x}_0 + \bar{e}_1)(\ell/R)\mu\cos\psi + \mu^2\sin^2\psi +2\mu\overset{*}{\bar{v}}(\ell/R)\sin\psi$$

$$+2\mu(\bar{x}_0 + \bar{e}_1)(\ell/R)\sin\psi + 2\overset{*}{\bar{v}}(\bar{x}_0 + \bar{e}_1)(\ell/R)^2 + (\bar{x}_0 + \bar{e}_1)^2(\ell/R)^2]$$

$$-\mu^2\cos^2\psi(v_{,x}w_{,x} + v_{,x}\beta_p)-\mu^2\sin\psi\cos\psi(w_{,x}+\beta_p)$$

$$-\mu\sin\psi[\lambda + w_{,x}\bar{v}(\ell/R) + \beta_p\bar{v}(\ell/R) + \overset{*}{w}(\ell/R)]$$

$$-\mu\cos\psi[w_{,x}\overset{*}{\bar{v}}(\ell/R) + \beta_p\overset{*}{\bar{v}}(\ell/R)+(w_{,x} + \beta_p)(\bar{x}_0 + \bar{e}_1)(\ell/R) +$$

$$\lambda v_{,x} + (\ell/R)\overset{*}{\bar{w}}\, v_{,x}]-\lambda\overset{*}{\bar{v}}(\ell/R)-\overset{*}{\bar{v}}\,\overset{*}{\bar{w}}(\ell/R)-\lambda(\bar{x}_0 + \bar{e}_1)(\ell/R)$$

$$-v(w_{,x} + \beta_p)(\bar{x}_0 + \bar{e}_1)(\ell/R)^2-\overset{*}{\bar{w}}(\bar{x}_0 + \bar{e}_1)(\ell/R)^2 +$$

$$+w_{,x}v_{,x}[\mu^2\sin^2\psi + 2\mu(\bar{x}_0 + \bar{e}_1)(\ell/R)\sin\psi +(\bar{x}_0 + \bar{e}_1)^2(\ell/R)^2]\}$$

$$+(0.5-\bar{x}_A)(1-\bar{x}_A)b(\overset{*}{\theta}_G + \overset{*}{\phi})[-\mu\sin\psi - (\ell/R)(\bar{x}_0 + \bar{e}_1)]\Big\rangle \tag{48}$$

$$\tilde{q}_{yA} = v_{,x}\tilde{q}_{xA} \tag{49}$$

$$\tilde{q}_{zA} = w_{,x}\tilde{q}_{xA} \tag{50}$$

Damping Loads which can represent the structural damping present in the system, or a certain amount of mechanical damping introduced by dampers, are assumed to be of a viscous type. As indicated above the equations are formulated in the $\hat{e}_x$,$\hat{e}_y$ and $\hat{e}_z$ system rotating with the blade, thus the damping loads are formulated in the same system

$$\underset{\sim}{p}_D = -q_{SL}\Omega\overset{*}{v}\,\hat{e}_y - q_{SF}\Omega\overset{*}{w}\,\hat{e}_z \tag{51}$$

Furthermore a distributed structural damping moment is also assumed to exist

$$\underset{\sim}{q}_D = - g_{ST}\,\Omega\overset{*}{\phi}\hat{e}_x \tag{52}$$

Final Equations of Motion in nonlinear partial differential form are presented below. These equations are obtained by performing the various algebraic manipulations for the inertia loads and application of the ordering scheme, together with the substitution of Eqs. (46) through (52) into

into Eqs. (4) through (7)

$$T_{,x} + \tilde{p}_{xI} = 0 \tag{53}$$

$$[E(I_2\cos^2\theta_G + I_3\sin^2\theta_G)v_{,xx} + E(I_2-I_3)\sin\theta_G\cos\theta_G(w_{,xx} -$$

$$-2\,v\phi_{,xx}) + E(I_2-I_3)\phi w_{,xx}\cos 2\theta_G]_{,xx} + (GJ\phi_{,x}w_{,xx})_{,x}$$

$$-(v_{,x}T)_{,x} + [2\Omega^{2*}\theta_G(I_{m2}-I_{m3})\sin\theta_G\cos\theta_G]_{,x}$$

$$-[m\Omega^2 x_I(x_0 + e_1)\cos\theta_G]_{,x} + m\dot{v} + 2m\Omega\dot{u} - 2m\Omega\beta_p\dot{w}$$

$$-mx_I\Omega^{2**}\theta_G\sin\theta_G - m\Omega^2 v - m\Omega^2 x_I\cos\theta_G + g_{SL}\dot{v} - \tilde{p}_{yA} = 0 \tag{54}$$

$$[E(I_2-I_3)\sin\theta_G\cos\theta_G(v_{,xx} + 2\phi w_{,xx}) + E(I_2-I_3)\phi v_{,xx}\cos 2\theta_G$$

$$+E(I_2\sin^2\theta_G + I_3\cos^2\theta_G)w_{,xx}]_{,xx} - (GJ\phi_{,x}v_{,xx})_{,x}$$

$$-(w_{,x}T)_{,x} - [mx_I\Omega^2(x_0 + e_1)\sin\theta_G]_{,x} + [2\Omega^{2*}\theta_G(I_{m2}\sin^2\theta_G +$$

$$I_{m3}\cos^2\theta_G)]_{,x} + mx_I\Omega^{2**}\theta_G\cos\theta_G + m\dot{w} + 2m\Omega\beta_p\dot{v} +$$

$$+m\Omega^2\beta_p(x_0 + e_1) + g_{SF}\dot{w} - \tilde{p}_{zA} = 0 \tag{55}$$

$$[GJ(\phi_{,x} + v_{,xx}w_{,x})]_{,x} + E(I_2-I_3)[\sin\theta_G\cos\theta_G(v_{,xx}^2 - w_{,xx}^2)$$

$$-v_{,xx}w_{,xx}\cos 2\theta_G]-g_{ST}\Omega\overset{*}{\phi}-\Omega\{(I_{m2}+I_{m3})(\overset{**}{\theta}_G+\overset{**}{\phi})$$

$$+mx_I\cos\theta_G[w_{,x}(x_0+e_1)-(x_0+e_1)v_{,x}\phi-\phi\overset{**}{v}+v\phi+\overset{**}{w}+\beta_p(x_0+e_1)$$

$$+2\overset{*}{v}(w_{,x}+\beta_p)]+mx_I\sin\theta_G[-v_{,x}(x_0+e_1)-\overset{**}{v}+v]$$

$$+I_{m2}[(1+2\overset{*}{v}_{,x})\sin\theta_G\cos\theta_G+(-\beta_p v_{,x}+2\overset{*}{v}_{,x}\phi+\phi+w_{,x}\overset{**}{v}_{,x})\cos^2\theta_G]$$

$$+I_{m3}[-(1+2\overset{*}{v}_{,x})\sin\theta_G\cos\theta_G+\phi\sin^2\theta_G+(2\overset{*}{v}_{,x}\overset{*}{w}_{,x}+$$

$$\overset{**}{v}_{,x}w_{,x}+2\overset{*}{w}_{,x}-2\phi\overset{*}{v}_{,x}-\phi+\beta_p v_{,x})\cos^2\theta_G]+\tilde{q}_{xA}=0 \qquad (56)$$

Where Eqs. (54) through (56) represent, respectively, the lag, flap and torsional equations of dynamic equilibrium. The exact boundary conditions corresponding to these equations are presented in Ref. 18. Within the context of the ordering scheme it can be shown[19] that these boundary conditions are equivalent to

$$v = w = v_{,x} = w_{,x} = 0 \text{ and } K_\phi\phi = GJ\phi_{,x} \text{ at } x_0 = 0$$

and $$v_{,xx} = v_{,xxx} = w_{,xx} = w_{,xxx} = \phi_{,x} = T = 0 \text{ at } x_0 = \ell$$

A number of comments regarding these equations should be made. First it is important to note that these equations are more consistent than the equations which have been used previously[7,13,24] because distinction between the deformed and undeformed state of the blade is carefully done. Distinction between the undeformed and deformed states is achieved by using a moderate deflection type of beam theory such as derived in Reference 18. Such a theory is a prerequisite for a consistent formulation of the inertia and aerodynamic loads.

Finally it should be mentioned that a careful comparison of these equations with Reference 13 is presented in Reference 19. The differences between the two sets of equations have been found to be quite small. (i.e. very few terms) when the same ordering scheme is applied to both sets of equations.

3. Solution of the Equations

3.1 Modal Substitution

The system of general, coupled, partial differential equations of motion presented in the previous section is transformed into a system of ordinary nonlinear differential equations by using Galerkin's method to eliminate the spatial variable. In this process the elastic degrees of freedom in the problem are represented by the uncoupled free vibration modes of a rotating blade. The elastic degrees of freedom w, v and ϕ are represented by

$$w = \sum_{i=1}^{n_F} \ell g_i(\psi) n_i(x_0)$$

$$v = \sum_{j=1}^{n_L} \ell h_j(\psi) n_j(x_0) \qquad (57)$$

$$\phi = \sum_{k=1}^{n_T} f_k(\psi) \phi_k(x_0)$$

The various algebraic details as well as the final equations are not presented in this paper and can be found in Reference 19.

3.2 Linearization and Solution of the Equations of Motion

The equations of motion described in the previous section are a system of coupled, nonlinear, ordinary differential equations with periodic coefficients. It is possible to obtain solutions to these equations by direct numerical integration, however in order to extract explicit information on the aeroelastic stability of the system, in terms of eigendata, the equations have to be linearized. In this paper the nonlinear differential equations of motion are linearized about a time dependent equilibrium position of the helicopter in forward flight [17,19,21,24] (See Figure 4.)

In order to simulate two possible configurations two different trim procedures are used:

(a) Propulsive Trim which simulates actual forward flight conditions. The weight coefficient (approximately equal to the thrust coefficient) is given and horizontal and vertical force equilibrium is maintained. In addition zero pitching and rolling moments on the rotor are maintained.

When using this trim procedure, μ and C_w are specified and θ_{1s}, θ_{1c}, θ_0, α_R and λ are computed from this trim procedure.

(b) Wind Tunnel or Moment Trim simulates conditions under which a rotor would be tested in the wind tunnel. Horizontal and vertical force equilibrium is not required for this case because the rotor is mounted on a supporting structure. Only the requirement of zero pitching and rolling moments on the rotor is imposed.

When using this trim procedure μ, θ_0 and α_R are specified and C_T, θ_{1s}, θ_{1c} and λ are computed from the trim procedure.

The details of these trim calculations together with the assumptions used can be found in References 21, 24. It should be noted that this trim calculation is somewhat different from a previous version used in Reference 17. The main difference is due to the fact that here direct aerodynamic moment considerations are used.

The linearized modal equations of motion are written as a set of perturbation equations about a time dependent equilibrium position arising from the cyclic pitch variations required to trim the rotor in forward flight[19]. The time dependent equilibrium position of the blade can be determined from various considerations, in this study, in order to keep this process reasonably simple some simplifying assumptions were made.

(a) In the calculation of the time dependent equilibrium position only the first harmonic terms are considered. Thus the time dependent equilibrium position is written as

$$\{\bar{q}(\psi)\} = \{q^0\} + \{q_{1c}\}\cos\psi + \{q_{1s}\}\sin\psi \qquad (58)$$

Furthermore while the modal equations were derived for an arbitrary number of modes, the actual number of modes for which results are obtained in this paper is limited to one mode for each elastic degree of freedom.

(b) For most cases an apprpximate time dependent equilibrium position is defined by neglecting combinations of the type $q_i^0 q_{1c}$, $q_1^0 q_{1sj}$ and $q_{1ci}q_{1cj}$, or higher combinations, for i, j-1,...,n, which are nonlinear combinations of terms defining the equilibrium position. For a limited number of cases the full nonlinear time dependent equilibrium position was used[19]. For this case determination of the nonlinear time dependent equilibrium position leads to the solution of a set of nonlinear algebraic equations for q_i^0, q_{1sj}, q_{1ci}...etc. These equations are solved by iterative methods similar to that described in Reference 7. It should be noted that more accurate, numerical, methods for calculating the time dependent equilibrium position could be implemented. It should be emphasized, however, that all calculations of an equilibrium position about which the

equations are linearized have to be approximate in one way or another, otherwise one attempts to solve directly the stability problem of the coupled nonlinear periodic system.

The process of linearization of the equations of motion consists of expressing the generalized coordinates by

$$\{q(\psi)\} = \{q(\bar{\psi})\} + \{\Delta q(\psi)\} \tag{59}$$

Substituting this expression into the nonlinear equations of motion and neglecting terms which contain squares of the perturbations $\Delta q_i(\psi)$ yields a second order, linear periodic system, which is rewritten in first order state variable form to yield

$$\{\overset{*}{y}\} = [A(\psi)]\ \{y\} \tag{60}$$

The stability investigation of this periodic system is based upon multivariable Floquet-Liapunov theory. The transition matrix at the end of one period is evaluated using an efficient numerical scheme[25] and the stability of the system is determined from the characteristic exponents

$$\lambda_k = \zeta_k + i\omega_k \tag{61}$$

The system is stable when $\zeta_k < 0$.

4. Results and Discussion

4.1 Assumptions and Numerical Values Used in the Computations

The equations of motion described in the present study are general and capable of simulating arbitrary blade configurations. However the results which are presented in this section were obtained by using a number of simplifying assumptions which were introduced primarily in order to facilitate the algebraic manipulations and the programming effort required to obtain these numerical results.

The most important simplifying assumptions are listed below:

(a) Mass and stiffness distributions were assumed to be constant along the span of the blade.

(b) Built-in twist θ_B was assumed to be zero

(c) Cyclic components of the inflow were assumed to be zero, i.e., $\lambda_{1c} = \lambda_{1s} = 0$.

(d) One rotating mode shape is used to represent each elastic degree of freedom. The fundamental rotating mode shapes in flap, lag and torsion, respectively, are uncoupled modes defined at zero pitch setting. Each of these modes is obtained by solving the appropriate free vibration problem by using Galerkin's method based upon five non-rotating appropriate modes of a uniform beam in bending or torsion. The integrals required for the solution of the free vibration problem are evaluated using sixteen point Gaussian integration.

(e) The various integrals resulting from application of Galerkin's method and associated with the structural inertia and aerodynamic operators are evaluated using seven point Gaussian integration.

Finally for all cases except when otherwise stated, on the plots illustrating the various results, the following numerical values were used in the calculations:

$$\alpha_R = \bar{x}_A = \gamma_F = \bar{k}_{m3} = \eta_{SF1} = \eta_{SL1} = \eta_{ST1} = 0$$

$$\bar{k}_{m2} = 0.02;\ (C_{d0}/a) = 0.0015915;\ C_{DP} = 0.01$$

$$a = 2\pi;\quad b = 0.0313;\ K_\phi = \infty \text{ (root torsion locked out)}$$

4.2 Results

The results presented in this section have two main objectives: (a) to show the effect of forward flight on the coupled flap-lag-torsional problem (b) to illustrate the importance of the nonlinear terms, due to moderate deflections, by considering similar blade configurations which are linearized about time dependent equilibrium positions based on different assumptions.

Figures 5 through 8 illustrate the effect of forward flight on the coupled flap-lag-torsional dynamics of the blade using an approximate, linearized, time dependent equilibrium position, obtained from the propulsive trim procedure. These figures illustrate the variation of the real part of the characteristic exponents associated with the flap, lag and torsional degrees of freedom, respectively. The values of ζ_k are shown as a function of the advance ratio μ for a number of blade configurations and loading conditions.

Figures 5 and 6 illustrate the behavior of a soft in-plane blade configuration under two loading conditions. For a very high weight coefficient (approximately equal to the thrust coefficient) $C_w = 0.01$, three configurations are shown corresponding respectively to a blade having very high, high

and an average amount of torsional stiffness. The case of $\bar{\omega}_{T1} = 15.033$ represents virtually the case of flap-lag in forward flight. The results clearly indicate that this configuration is significantly destabilized by introducing the torsional degree of freedom. However at the same time it is important to note that the degree of freedom which becomes unstable is the lag degree of freedom. As shown in the figure the value of μ_{cr} at which the blade can become unstable is very sensitive to the amount of torsional stiffness present in the system.

Figure 5 can be also used to illustrate the effect of forward flight on the coupled flap-lag-torsional dynamics of the blade. At $\mu = 0$, which represents hover the blade is stable, propulsive trim at such high values of C_w introduces significant changes in the collective and cyclic pitch requirements resulting in a less stable blade configuration. Thus it is important to realize that the combination of the trim requirement due to forward flight is the primary source of the degradation in aeroelastic stability due to forward flight.

Figure 6 illustrates a similar blade configuration under a much more reasonable loading condition represented by $C_w = 0.005$. As shown the results for this case are much less sensitive to the gradual introduction of the torsional degree of freedom. At the same time the degradation in stability associated with forward flight effects is still clearly evident.

Figures 7 and 8 illustrate the behavior of a stiff inplane blade under two loading conditions. Figure 7 shows the behavior of this configuration under high loads, $C_w = 0.01$, as indicated by the plots this configuration is less sensitive to the gradual introduction of the torsional degree of freedom. Again the degradation in the aeroelastic stability margins, due to the introduction of effects associated with forward flight is clearly evident from the figure.

Figure 8 illustrates the behavior of this configuration at a much lower thrust coefficient, $C_w = 0.005$ for this case the lower collective pitch setting required reduces the values of the characteristic exponents associated with the lag degree of freedom. This is a result of a reduction in aerodynamic damping in the lag degree of freedom which contains a term proportional to θ_0. As shown, this configuration is quite sensitive to both the amount of torsional stiffness and the effects associated with forward flight.

It is also interesting to note that for all cases considered in Figures 5 through 8, the degree of freedom which becomes unstable is the lead-lag degree of freedom. Clearly this behavior is due to the inherently low aerodynamic damping present in this degree of freedom and its sensitivity to destabilizing inertia, aerodynamic and structural coupling effects.

Figures 9 and 10 illustrate the combined effect of lock number and blade loading on the coupled flap-lag-torsional dynamics in forward flight. Comparing Figures 7 and 9 indicates that the results and conclusions shown

in Figure 7 are relatively insensitive to a significant reduction in γ. The effect of decreasing the blade loading to $C_w = 0.005$ is illustrated by Figure 10. Comparing Figures 9 and 10 clearly illustrates that for lower loading the configuration is more stable in forward flight. Comparing Figures 8 and 10 indicates that for lower loading, $C_w = 0.005$, the configuration is more sensitive to a reduction in lock number. The combined effect of torsion and forward flight is similar to the trends shown in the previous figures.

Figure 11 illustrates the sensitivity of the results to the trim procedure, or to be more precise the time dependent equilibrium position determined by the trim procedure. Figure 11 should be compared to Figure 8, the value of $\theta_0 = 0.1705$ was chosen so as to correspond approximately to $C_w = 0.005$. From the sensitivity of the results to variations in torsional stiffness it is evident that the effect of forward flight for this case is quite different from the behavior shown in Figure 8, thus for the case of moment trim there is much less degradation in stability with forward flight. The different behavior is due to the difference in equilibrium position about which the equations are linearized, this reiterates the importance of including the terms associated with moderate deflections in the equations of motion. Another interesting aspect of these results is due to the fact that the moment trim condition simulates blade behavior under conditions resembling a wind tunnel test while propulsive trim simulates actual forward flight behavior. These results indicate that wind tunnel tests conducted on a rotor, have to be carefully interpreted before drawing conclusions regarding blade behavior in actual forward flight.

Figure 12 and 13 taken from Reference 24 are included in order to emphasize a similar aspect of the problem. The forward flight results presented in this paper are based upon an approximate linearized equilibrium position which has been defined in Section 3.2. In reality a more accurate nonlinear time dependent equilibrium position can be obtained where nonlinear combinations in q_{1s}, q_{1c}...etc. are retained. The effect of such a more accurate equilibrium position for the case of coupled flap-lag dynamics in forward flight, is illustrated in Figures 12 and 13. The effect of the nonlinear equilibrium position for the case of a soft in-plane blade configuration is depicted in Figure 12, at a high collective pitch setting. Figure 12 illustrates very well the fact that the use of a nonlinear time dependent equilibrium position for this particular case significantly lowers blade stability in lead-lag when compared to the results based upon the approximate linear time dependent equilibrium position. For the stiff in-plane blade the use of the nonlinear time dependent equilibrium position affects the characteristic exponents for lead-lag and flap in a different manner. For this case, as shown in Figure 13, the nonlinear equilibrium position changes the critical degree of freedom, from lag to flap, the lag degree of freedom is stable and its characteristic exponent is not shown. However the solution based upon the linearized equilibrium position appears to be less stable than the one based on the nonlinear time dependent equilibrium position. Similar results are in the process of being generated for the coupled flap-lag-torsional case in forward flight[19].

Figure 14 illustrates the effect of the offset between the elastic axis and the aerodynamic center of the blade for the case of forward flight. The effect of this offset has been documented in the literature for the case of hover[7], its effect in the presence of forward flight is relatively unknown. Three offsets are compared in Figure 14 $\bar{x}_A = 0$, $\bar{x}_A = 0.05$ (2.5% of chord) and $\bar{x}_A = 0.10$ (5% of chord). As shown the $\bar{x}_A$ offset affects the flap and torsional degrees of freedom significantly, while its effect on the lag degree of freedom is minor. Additional results[19] not presented here indicate similar trends.

A number of concluding comments on the results presented in this paper are in order. First a comparison of these results obtained with results presented in Reference 16 indicate similar trends. Numerical differences between the results are evident. These differences are due to some extent to the improved set of equations employed in this paper. Secondly it is important to note that blade behavior in forward flight will probably be considerably affected by compressibility and time dependent and spatially dependent inflow such as stipulated in Eq. (2). These effects however were neglected in the numerical results. Next it is important to note that studies of aeroelastic stability in hover have indicated[1], that two or three modes for each elastic degree of freedom should be used to get good convergence. These results based upon a single mode representation for each elastic degree of freedom can be considered to be indicative of trends only.

5. Conclusions

The main conclusions obtained in the present study are summarized below. They should be considered to be indicative of trends and their application to the design of a helicopter blade should be limited by the assumptions used in obtaining the numerical results presented in this study.

(1) Coupled flap-lag-torsional analyses in hover, without precone and with typical values of bending and torsion frequencies, indicate generally stable configurations for practical values of collective pitch settings. Effects associated with forward flight and consequent trim requirements can bring about a significant degradation in the aeroelastic stability margins computed for hover.

(2) Small amounts of offset between elastic axis and aerodynamic center do not seem to affect blade stability in forward flight.

(3) Effect of the moderate deflections is significant for blade stability in forward flight as indicated by the sensitivity of the stability boundaries to the time dependent equilibrium position about which the equations are linearized.

References

1. Friedmann, P., "Recent Developments in Rotary-Wing Aeroelasticity," Paper No. 11, Proceedings of Second European Rotorcraft and Powered Lift Aircraft Forum, Buckeburg, Federal Republic of Germany, September 1976, pp. 11.1-11.33. (to be published in J. of Aircraft, Nov. 1977).

2. Burkham, J.E. and Miao, W., "Exploration of Aeroelastic Stability Boundaries with a Soft-in Plane Hingeless Rotor Model," J. American Helicopter Society 17, No. 4, p. 27-35, October 1972.

3. Friedmann, P. and Tong, P., "Dynamic Nonlinear Elastic Stability of Helicopter Rotor Blades in Hover and in Forward Flight," NASA CR-114 485, also MIT Aeroelastic and Structures Research Lab., TR 166-3, June 1972.

4. Hodges, D.H. and Ormiston, R.A., "Stability of Elastic Bending and Torsion of Uniform Cantilevered Rotor Blades in Hover," AIAA Paper No. 73-405, April 1973.

5. Huber, H.B., "Effect of Torsion-Flap-Lag Coupling on Hingeless Rotor Stability," AHS Preprint No. 731, Presented at the 29th Annual National Forum of the American Helicopter Society, Washington, D.C., May 1973.

6. Houbolt, J.C. and Brooks, G.W., "Differential Equations for Combined Flapwise Bending, Chordwise Bending and Torsion of Twisted Non-uniform Rotor Blades," NACA Report 1346, 1958.

7. Friedmann, P., "Influence of Modeling and Blade Parameters on the Aeroelastic Stability of a Cantilevered Rotor," AIAA Journal, Vol. 15, No. 2., February 1977, pp. 149-158.

8. Hodges, D.H. and Dowell, E.H., "Nonlinear Equations of Motion for the Elastic Bending and Torsion of Twisted Nonuniform Rotor Blades," NASA TN D-7818, December 1974.

9. Hodges, D.H. and Ormiston, R.A., "Stability of Elastic Bending and Torsion of Uniform Cantilever Rotor Blades in Hover with Variable Structural Coupling," NASA TN D-8192, April 1976.

10. Hodges, D.H. and Ormiston, R.A., "Stability of Hingeless Rotor Blades in Hover with Pitch-Link Flexibility," AIAA Journal, Vol. 15, No. 4, April 1977, pp. 476-482.

11. Bielawa, R.L., "Aeroelastic Analysis of Helicopter Rotor Blades with Time Variable, Nonlinear Structural Twist and Multiple Structural Redundancy, Mathematical Derivation and Program User's Manual," NASA CR-2638, May 1976.

12. Bielawa, R.L., "Aeroelastic Characteristics of Composite Bearingless Rotor Blades," AHS Preprint No. 1032, Presented at the 32nd Annual National V/STOL Forum of the American Helicopter Society, Washington, D.C., May 1976.

13. Reyna-Allende, M., "The Coupled Flap-Lag-Torsional Aeroelastic Stability of Helicopter Rotor Blades in Forward Flight," Ph.D. Thesis, Mechanics and Structures Department, University of California, Los Angeles, November 1976.

14. Hodges, D.H., "Nonlinear Equations of Motion for Cantilevered Rotor Blades in Hover with Pitch Link Flexibility, Twist, Precone, Droop, Sweep, Torque Offset and Blade Root Offset," NASA TMX-73, May 1976.

15. Powers, R.W., "A Study of Several Approximation Concepts in Rotary-Wing Aeroelasticity," M.S. Thesis, Mechanics and Structures Department, University of California, Los Angeles, June 1976.

16. Friedmann, P. and Reyna-Allende, M., "Aeroelastic Stability of Coupled Flap-Lag-Torsional Motion of Helicopter Rotor Blades in Forward Flight," AIAA Paper No. 77-455, presented at the AIAA Dynamics Specialist Conference, San Diego, and published in Vol. B - A Collection of Technical Papers on Dynamics, Structural Dynamics, March 1977, pp. 314-326.

17. Friedmann, P. and Shamie, J., "Aeroelastic Stability of Trimmed Helicopter Blades in Forward Flight," First European Rotorcraft and Powered Lift Aircraft Forum, University of Southampton, September 1975 published in Vertica - The International Journal of Rotorcraft and Powered Lift Aircraft, Vol. 1, No. 3, 1977, pp. 189-211.

18. Rosen, A. and Friedmann, P., "Nonlinear Equations of Equilibrium for Elastic Helicopter or Wind Turbine Blades Undergoing Moderate Deformation," University of California, Los Angeles, School of Engineering and Applied Science Report, UCLA-ENG-7718, January 1977 (Revised June 1977).

19. Shamie, J. and Friedmann, P., "Coupled Flap-Lag-Torsional Dynamics of Helicopter Rotor Blades in Forward Flight," University of California, Los Angeles, School of Engineering and Applied Science Report, to be published in 1977.

20. Friedmann, P. and Yuan, C., "Effect of Modified Aerodynamic Strip Theories on Rotor Blade Aeroelastic Stability," AIAA Journal, Vol. 15, No. 7, July 1977, pp. 932-940.

21. Shamie, J. and Friedmann, P., "Aeroelastic Stability of Complete Rotors with Application to a Teetering Rotor in Forward Flight," Journal of Sound and Vibration, Vol. 53, No. 4, August 1977.

22. Meirovitch, L., "Methods of Analytical Dynamics," McGraw-Hill, 1970.

23. Bisplinghoff, R.L., Ashley, H. and Halfman, R.L., "Aeroelasticity," Addison-Wesley Co., 1955.

24. Shamie, J., "A Study of the Aeroelastic Stability of Complete Rotors with Application to a Teetering Rotor in Hover and Forward Flight," Ph.D. Thesis, Mechanics and Structures Department, School of Engineering and Applied Science, University of California, Los Angeles, July 1976.

25. Friedmann, P., Hammond, C.E. and Woo, T., "Efficient Numerical Treatment of Periodic Systems with Application to Stability Problems," International Journal of Numerical Methods in Engineering, Vol. 11, No. 7, July 1977, pp. 1117-1136.

Appendix A. List of Symbols

$[A(\psi)]$ = periodic matrix used in the state variable formulation of the aeroelastic stability problem given in Reference 19

a = two-dimensional lift-curve slope

$\bar{a}$ = acceleration vector

A = cross sectional area of the blade

b = semi-chord, nondimensionalized with respect to R

$C(k)$ = Theodorsen's lift deficiency function

$C_W = W/\rho_A \pi (R\Omega R)^2$ = weight coefficient

$C_T = \bar{T}/\rho_A \pi (R\Omega R)^2$ = thrust coefficient

$C_H = \bar{H}/\rho_A \pi (R\Omega R)^2$ = horizontal force coefficient

C_{d0} = profile drag coefficient

C_{DP} = parasite drag coefficient

D_P = parasite drag of the helicopter

e_1 = offsets of the blade root from the axis of rotation, shown in Fig. 2

$\hat{e}_x, \hat{e}_y, \hat{e}_z$ = unit vectors in the directions of the coordinates x_0, y_0, z_0, respectively before the deformation

$\hat{e}'_x, \hat{e}'_y, \hat{e}'_z$ = the triad $\hat{e}_x, \hat{e}_y, \hat{e}_z$ after the deformation

$\hat{e}''_x, \hat{e}''_y, \hat{e}''_z$ = triad defined by Eqs. (37)

E = Young's Modulus

$f_k(\psi)$ = generalized coordinates for ϕ degree of freedom

$g_i(\psi)$ = generalized coordinates for w degree of freedom

GJ = torsional stiffness of the blade

g_{SF}, g_{SL}, g_{ST} = viscous structural damping coefficients in flap, lag and torsion respectively

$\dot{h}$ = plunging velocity, in Theodorsen's theory

$h_j(\psi)$ = generalized coordinates for v degree of freedom

I_2, I_3 = principal moments of inertia of the cross section

$\underset{\sim}{i}, \underset{\sim}{j}, \underset{\sim}{k}$ = unit vectors in the directions x,y and z, respectively

I_b = flapping mass moment of inertia of blade about its root

$I_{m2}, I_{m3} (= k^2_{m2} m, k^2_{m3} m)$ = given by $I_{m2} = \int_A \rho \eta^2 dA$; $I_{m3} = \int_A \rho \zeta^2 dA$

i = $\sqrt{-1}$

K_ϕ = root torsional spring stiffness

$k_1(x), k_2(x), k_3(x)$ = arbitrary functions governing the spatial distribution of the inflow components

$k_{m2}, k_{m3} (\bar{k}_{m2}, \bar{k}_{m3})$ = radii of gyration of cross sectional mass; bars indicate nondimensionalization w.r.t. ℓ

k = reduced frequency ($\omega b R / V_0$)

L_Q = quasisteady lift, per unit span, in Theodorsen's theory

L = unsteady lift, per unit length, according to Theodorsen's theory

ℓ = length of elastic part of the blade

M = unsteady moment, per unit span, according to Theodorsen's theory

$\bar{p}$ = distributed external force vector per unit length of the axis of the blade, subscripts I, A and D represent inertia, aerodynamic and damping contributions, respectively

$\tilde{p}_x, \tilde{p}_y, \tilde{p}_z$ = components of the distributed external force in the directions $\hat{e}_x, \hat{e}_y$ and $\hat{e}_z$ respectively, subscripts I and A denote inertia and aerodynamic contributions respectively

p''_{zA}, p''_{yA} = aerodynamic loads per unit length in the $\hat{e}''_z$ and $\hat{e}''_y$ directions, respectively

$\bar{q}$ = distributed external moment vector per unit length along the axis of the blade, subscripts I, A and D represent inertia, aerodynamic and damping contributions, respectively

$\tilde{q}_x, \tilde{q}_y, \tilde{q}_z$ = components of $\bar{q}$ in the $\hat{e}_x, \hat{e}_y$ and $\hat{e}_z$ directions respectively, subscripts I and A represent inertia and aerodynamic contributions respectively

$\{q(\psi)\}$ = vector of generalized coordinates, having a number of elements equal to the number of elastic degrees of freedom (=n)

$\{\bar{q}(\psi)\}$ = vector defining time dependent equilibrium position of the blade

$\{q_{1c}\}, \{q_{1s}\}$ = cyclic components of $\{\bar{q}(\psi)\}$

$\{q^0\}$ = constant part of $\{\bar{q}(\psi)\}$

$\{\Delta q(\psi)\}$ = perturbation vector of $\{q(\psi)\}$ about $\{\bar{q}(\psi)\}$

q''_{xA} = aerodynamic moment, per unit length in the $\hat{e}'_x$ direction

R = blade radius

$\bar{R}$ = position vector of a mass point in the blade cross section, from the axis of rotation

$\bar{R}_p$ = position vector of a mass point in the blade cross section, from the elastic axis

$\bar{R}_{EA}$ = position vector of a point on the elastic axis of the blade, from the axis of rotation

S_{ij} = elements of the matrix which describes the transformation between the triads $(\hat{e}_x,\hat{e}_y,\hat{e}_z)$ and $(\hat{e}'_x,\hat{e}'_y,\hat{e}'_z)$

T = component of the resultant force which acts in the $\hat{e}'_x$ direction (axial tension)

$\bar{T}$ = average thrust used in trim calculations

u,v,w = components of the displacement $\bar{W}$ of a point on the elastic axis of the blade in the direction $\hat{e}_x,\hat{e}_y$ and $\hat{e}_z$, respectively

$\underset{\sim}{U}$ = total velocity vector at the elastic axis of the blade

U'_x,U'_y,U'_z = velocity vector components in the $\hat{e}'_x,\hat{e}'_y,\hat{e}'_z$ system

U''_x,U''_y,U''_z = velocity vector components in the $\hat{e}''_x,\hat{e}''_y,\hat{e}''_z$ system

V = velocity of forward flight of the helicopter

$\underset{\sim}{V}_{EA}$ = velocity vector of a point on the elastic axis of the blade

$\underset{\sim}{V}_A$ = contribution to the velocity vector, at the elastic axis, due to forward flight and inflow

V_0 = oncoming free stream velocity, in Theodorsen's theory

x,y,z = rotating coordinate system (Figure 2)

$\bar{x}$ = (x/ℓ)

x_0,y_0,z_0 = initial coordinate system of the blade (Figure 2)

$x_A,(\bar{x}_A=x_A/bR)$ = blade cross-sectional aerodynamic center offset from elastic axis, shown in Figure 3; positive for A.C. before E.A.

x_I = blade cross-sectional mass center of gravity from the elastic axis, shown in Figure 3; positive when in the positive direction of η.

x_{II} = offset between the elastic axis and tension center of the cross section of the blade; positive when in the positive direction of η

$\{y\}$ = state variable vector, having 2n elements, where n is the total number of degrees of freedom

Greek Symbols

α_R = angle of attack of the whole rotor

α = harmonic pitching angle used in Theodorsen's theory

β_P = preconing, inclination of the feathering axis with respect to the hub plane measured in a vertical plane

γ = $(2\ \rho_A b R^5 a)/I_b$; lock number

γ_F = flight path angle measured from horizontal

$\gamma_j(x_0)$ = shape functions for v degree of freedom

ϵ_D = symbolic quantity having the same order of magnitude as the elastic slopes of the blade

ζ_k = real part of the k-th characteristic exponent

$\eta_{SF1}, \eta_{SL1}, \eta_{ST1}$ = viscous structural damping coefficients in percent of critical damping, for the flap, lag and torsional mode respectively

η, ζ = cross-sectional coordinates, see Figure 3

$\eta_i(x_0)$ = shape functions for w degree of freedom

θ_r = total pitch angle, nonelastic, at pitch bearing about feathering axis

$\theta_B(x)$ = blade pretwist, built-in about elastic axis

θ_0 = collective pitch angle

θ_{1s}, θ_{1c} = cyclic pitch components

θ_c = critical value of collective pitch angle at which the linearized system becomes unstable in hover

λ_0 = constant part of the inflow ratio

$\lambda_{1s}, \lambda_{1c}$ = cyclic components of the inflow ratio

λ_k = characteristic exponent associated with the kth degree of freedom

$\mu = V \cos\alpha_R/\Omega R$ = advance ratio

μ_{cr} = critical value of the advance ratio at which the system becomes unstable

ρ = density of blade material

ρ_A = density of air

σ = blade solidity ratio; blade area/disk area

ϕ = the rotation of a cross section of the blade around the elastic axis

ϕ_R = root torsional elastic deformation, occurs about feathering axis

$\phi_D(x)$ = spanwise distributed torsional elastic deformation, occurs about elastic axis

$\phi_k(x_0)$ = shape functions for ϕ degree of freedom

ψ = azimuth angle of blade ($\psi=\Omega t$) measured from straight aft position

ω_k = imaginary part of the kth characteristic exponent

$\bar{\omega}_{F1}, \bar{\omega}_{L1}, \bar{\omega}_{T1}$ = first rotating natural frequencies in flap, lag and torsion respectively, nondimensionalized w.r.t. Ω

Ω = speed of rotation

$\bar{\Omega}$ = angular velocity vector

Special Symbols

$(^*)$ = differentiation with respect to ψ

$(\ )_{,x}$ = differentiation with respect to x_0

$(\hat{\ })$ = unit vector

$(\bar{\ }), (\underset{\sim}{\ })$ = vector

$(\underset{\sim}{\ }) \times (\underset{\sim}{\ })$ = vector cross product

Acknowledgment

The authors would like to acknowledge the generous help of W. Warmbrodt in preparing this paper together with the assistance of J. Treger and F. Straub in generating numerical results. Finally, we wish to thank Ms. D. Haines for her expeditious typing.

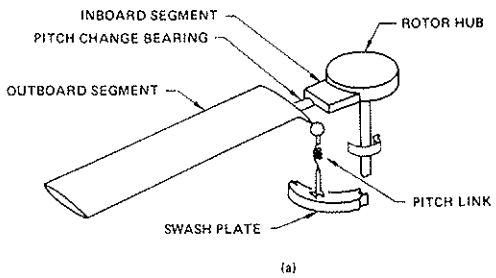

Figure 1a. Elements of a Typical Hingeless Rotor Blade

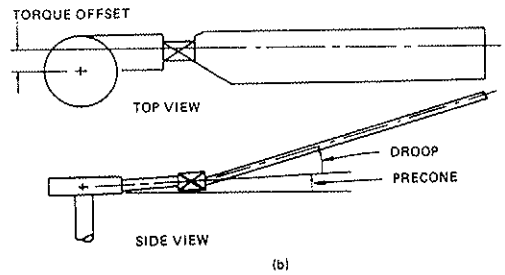

Figure 1b. Configuration Parameters of a Hingeless Rotor Blade

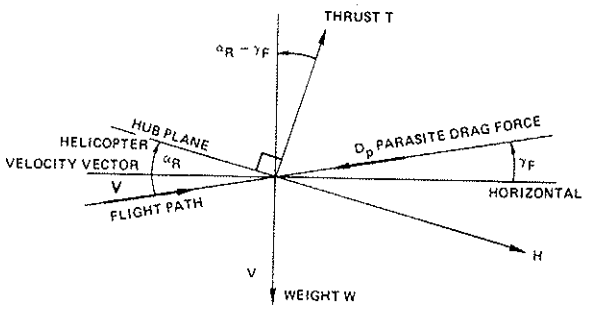

Figure 4. Geometry for the Trim Calculation

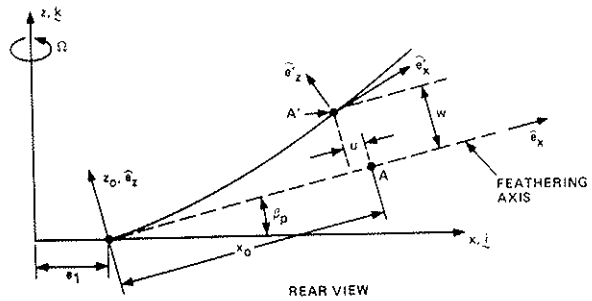

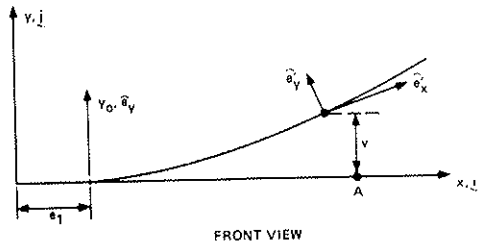

Figure 2b. Geometry of the Elastic Axis of the Deformed Blade

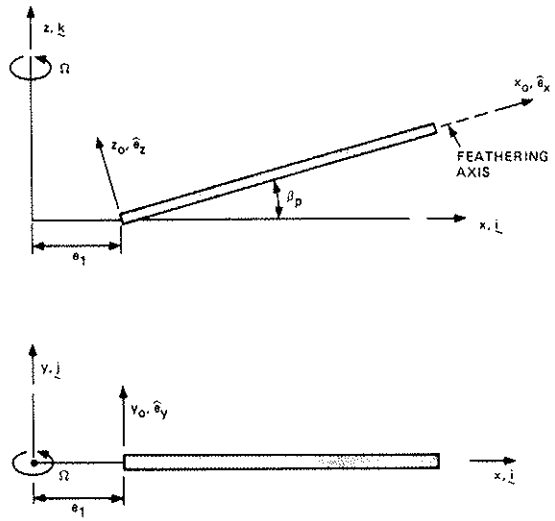

Figure 2a. Typical Description of the Undeformed Blade in the Rotating System x,y,z ($\underset{\sim}{i}$,$\underset{\sim}{j}$,$\underset{\sim}{k}$)

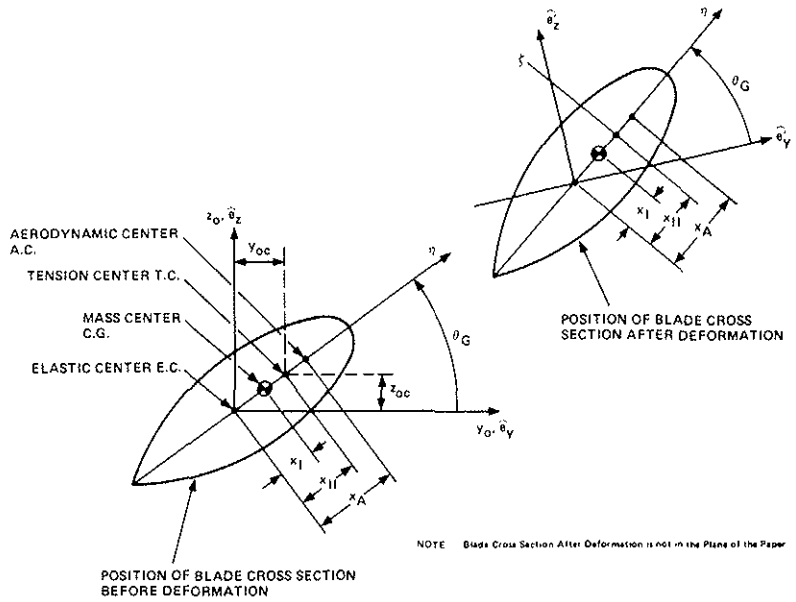

Figure 3. Blade Cross Section Positions Before and After the Deformation

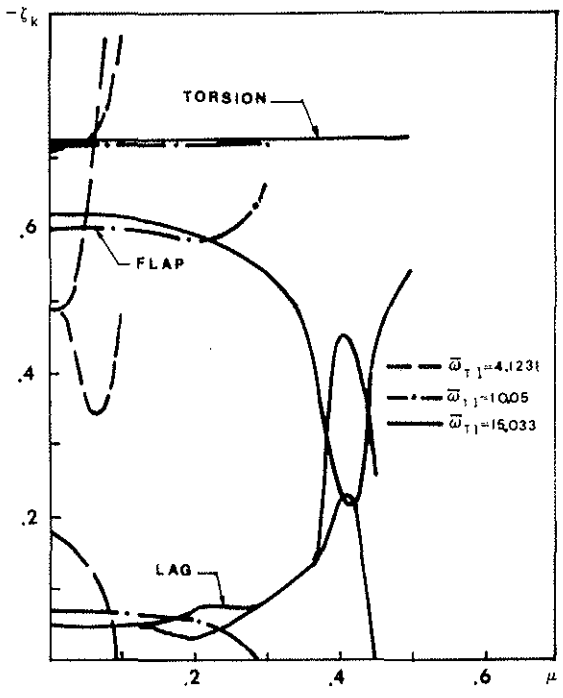

Figure 5. Real Part of Characteristic Exponents vs. μ (Propulsive Trim, C_W = 0.01; $\bar{\omega}_{F1}$ = 1.1006; $\bar{\omega}_{L1}$ = 0.90225; γ = 10; σ = 0.05)

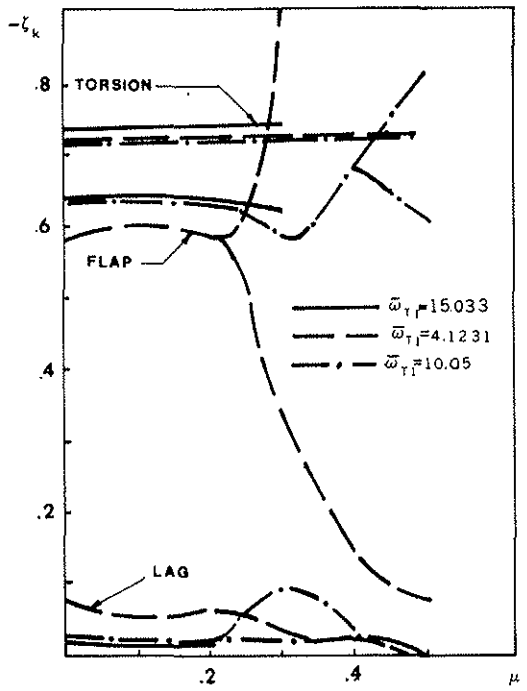

Figure 6. Real Part of Characteristic Exponents vs. μ (C_W = 0.005, all other data identical to Fig. 5)

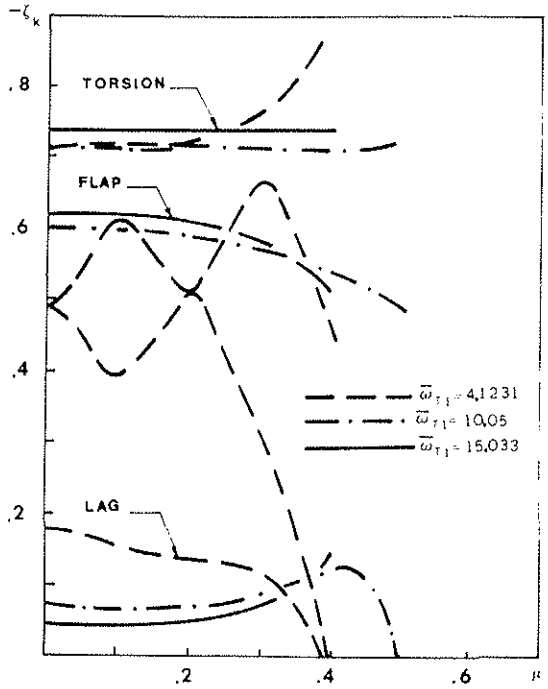

Figure 7. Real Part of Characteristic Exponents for Flap, Lag and Torsion vs. Advance Ratio (Propulsive Trim; $C_w = 0.01$; $\bar{\omega}_{F1} = 1.08238$ $\bar{\omega}_{L1} = 1.4171$; $\gamma = 10$; $\sigma = 0.05$)

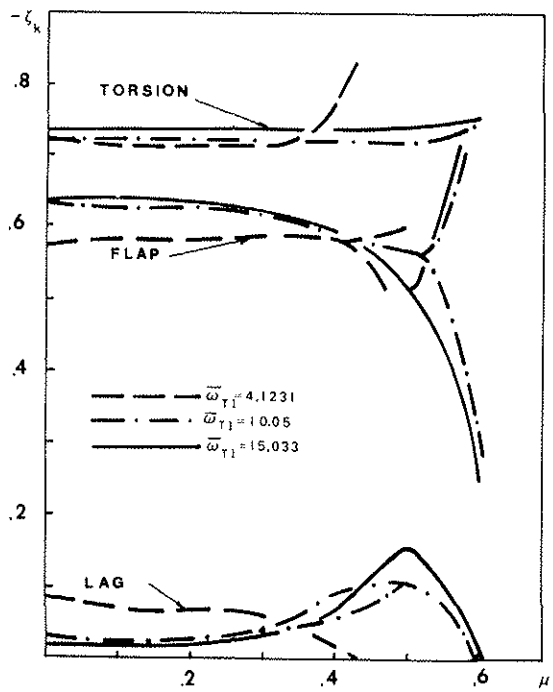

Figure 8. Real Part of Characteristic Exponents for Flap, Lag and Torsion vs. Advance Ratio (Propulsive Trim; $C_w = 0.005$; all other data identical to Fig. 7)

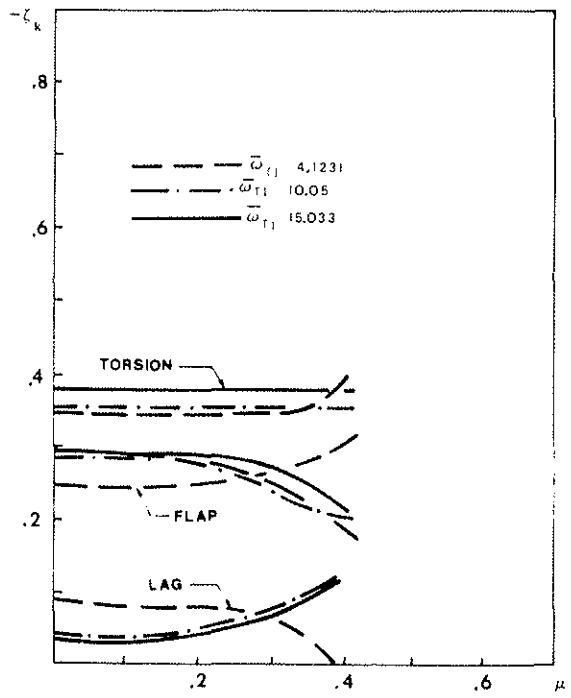

Figure 9. Combined Effect of Lock Number and Blade Loading on a Stiff In-plane Configuration (Propulsive Trim, C_W = 0.01, γ = 5, all other data identical to Fig. 7)

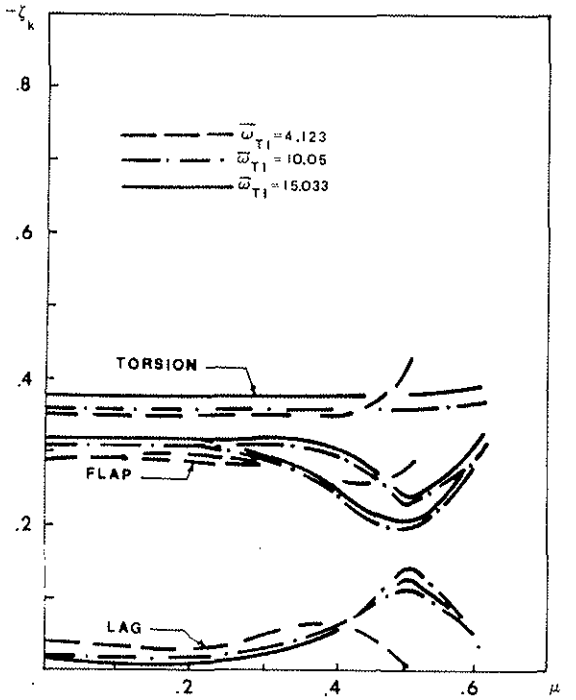

Figure 10. Combined Effect of Lock Number and Blade Loading on a Stiff In-plane Configuration (Propulsive Trim, C_W = 0.005, all other data identical to Fig. 9)

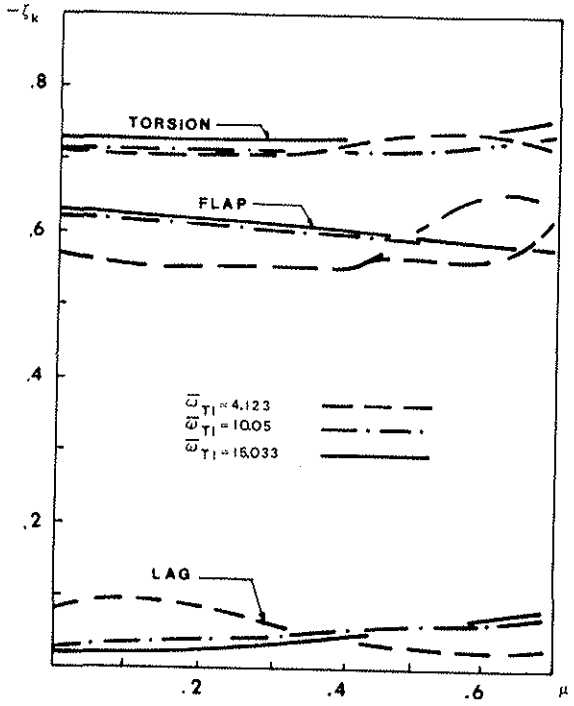

Figure 11. Effect of Trim Procedure on Blade Stability (Moment Trim, $\theta_0 = 0.1705$, all other data identical to Fig. 10)

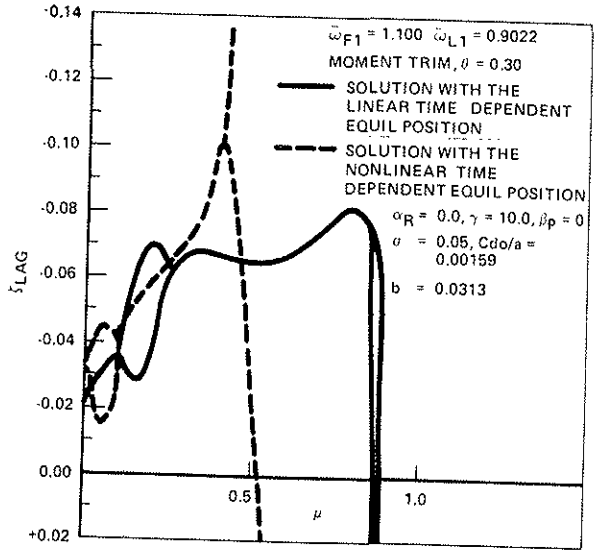

Figure 12. Effect of Nonlinear Time Dependent Equilibrium Position on the Flap-Lag Stability of a Soft In-plane Blade

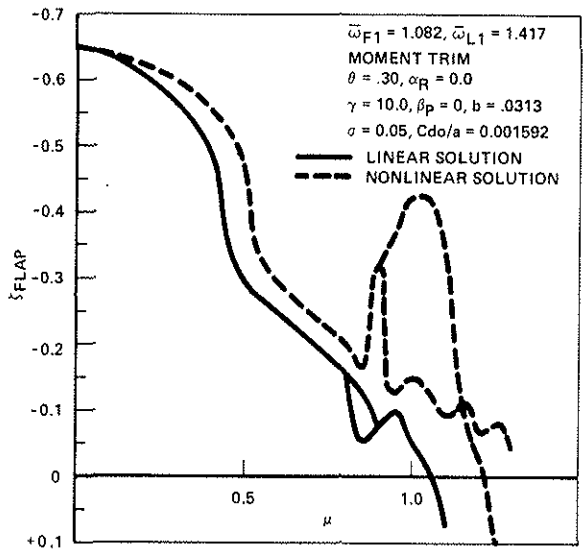

Figure 13. Effect of Nonlinear Time Dependent Equilibrium Position on a Stiff In-plane Blade

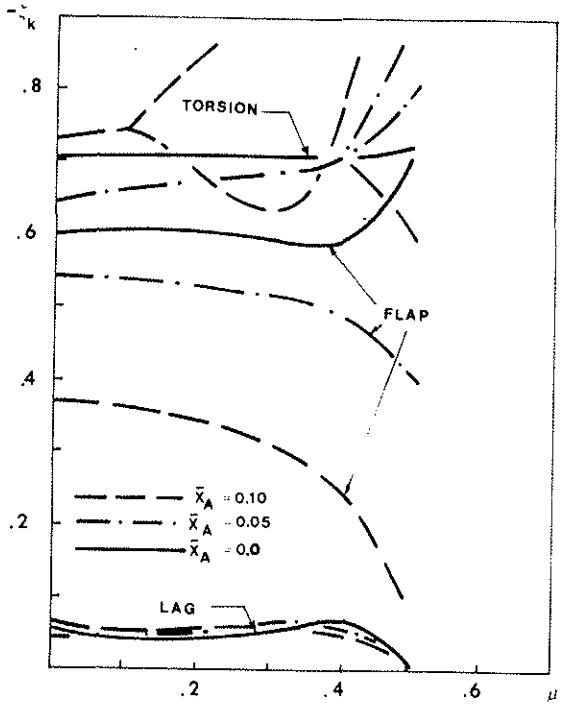

Figure 14. Combined Effect of $\bar{x}_A$ Offset and μ (Propulsive Trim, $\bar{\omega}_{F1} = 1.082$ $\bar{\omega}_{L1} = 1.4171$, $\bar{\omega}_{T1} = 6.083$; $\sigma = 0.05$; $\gamma = 10.$; $C_W = 0.005$)